Available online at www.sciencedirect.com
SCIENCE DIRECT®
International Journal of Heat and Mass Transfer 48 (2005) 145–160
International Journal of HEAT and MASS TRANSFER
www.elsevier.com/locate/ijhmt

Convection in modulated thermal gradients and gravity: experimental measurements and numerical simulations

Y. Shu, B.Q. Li *, B.R. Ramaprian

School of Mechanical and Materials Engineering, Washington State University, P.O. Box 642920, Pullman, WA 99164, United States

Received 8 December 2003; received in revised form 6 April 2004
Available online 12 October 2004

Abstract

This paper presents an investigation on natural convection in a cavity with imposed modulated thermal gradients or modulated gravity forces. Numerical computations are presented, which are based on the finite element solution of the transient Navier–Stokes and energy balance equations, along with appropriate thermal boundary conditions or time-varying gravity forces. In parallel with numerical development, an experimental system is setup where oscillating wall temperatures are prescribed to produce modulated temperature gradients and the velocity fields are measured by a laser-based particle image velocimetry (PIV) system. Computed results compare well with experimental measurements for various conditions. With the mathematical model, so verified by experimental measurements, numerical simulations are carried out to study the effects of modulation frequency and Prandtl number on the fluid flow. Results show strong non-linear interaction in a fluid with a relative high Prandtl number within the intermediate range of modulated frequency. It is also found that for a fluid with a small Prandtl number typical of molten metals and semiconductor melts, modulated gravity and thermal gradients produce almost the same flow field both in structure and in magnitude.

1. Introduction

Convection in modulated gravity and thermal gradients has been a subject of interest in the research community for the last several decades. Gershuni and Zhukhovitskii [1] were among the early investigators to study the instability of thermal convection driven by periodically varying parameters in idealized systems. Linear analysis of Bénard convection was also studied by Venezian [2] for a small amplitude modulation of boundary temperatures. Roppo et al. [3] studied the same problem with an oscillating wall temperature condition but their investigations also included weakly non-linear stability analyses. Pattern formation of a fluid layer driven by vertical temperature or gravity oscillations was investigated experimentally and numerically recently [4,5]. Weakly non-linear finite amplitude convection was also studied by several authors [6–10], whose analyses all have established that the onset of convection is altered under the modulation of constraints [11–16]. All these publications have been concerned with the convection stability of a horizontal layer extending to infinity subject to oscillating body forces that are either derived from gravity modulations or thermal gradient oscillations.

Several studies have also appeared on convection driven by modulated thermal gradients in systems of finite dimension. Kazmierczak and Chinoda [17] presented a finite volume solution of a laminar buoyancy-driven flow in a square cavity subject to an oscillating thermal

* Corresponding author.
E-mail address: li@mme.wsu.edu (B.Q. Li).

0017-9310/$ - see front matter © 2004 Elsevier Ltd. All rights reserved.
doi:10.1016/j.ijheatmasstransfer.2004.08.010

Nomenclature

A	non-dimensional amplitude of velocity after Fourier transformation
D	depth of the cavity
e	vertical unit vector
f	modulation frequency
g	gravity perturbation
$\mathbf{g}_0$	terrestrial gravity
g	amplitude of gravity oscillation
Gr	Grashoff number, $Gr_T = g^*\beta_T\Delta T^*L^{*3}/\nu^2$
H	height of the cavity
L	width of the cavity
p	pressure
Pr	Prandtl number, $Pr = \nu/\alpha$
St	Strouhal number, $St = \varpi L^*/u_0$
t	time
T	temperature
T_1, T_2	temperature at right and left sidewall
ΔT	temperature difference between two sidewalls
u	dimensionless velocity
u_0	convection velocity scale factor in the numerical simulation, $u_0 = \sqrt{g^*\beta\Delta T^*L^*/Pr}$ (m/s)
U_{max}	absolute value of maximum velocity
x, y	horizontal and vertical coordinates of the system

Greek symbols

α	thermal diffusivity (m^2/s)
β_T	thermal expansion coefficient (1/K)
ρ	density (kg/m^3)
ρ_0	density scale (kg/m^3)
ν	kinematic viscosity (m^2/s)
ϖ	oscillation frequency, $\varpi = 2\pi f^*$ (1/s)

Superscript

*	dimensional quantity

gradient. They showed that the transient flows become periodic in time with temperature oscillation, but the cycle-averaged heat flux across the cavity is insensitive to the temperature modulation at the boundaries. Kwak and Hyun [18,19] studied the resonance of natural convection in a square cavity in sinusoidal temperature fields using a finite volume method. The Nusselt numbers were calculated with various amplitudes and frequencies of temperature modulation for fixed Ralyleigh number and Prandtl number. They concluded that the time–mean heat transfer rate is largely dependent on the imposed temperature modulation in the cavity.

Numerical and analytical study on a different type of periodic thermal boundary condition was also conducted [20–26]. Lage and Bejan [20] studied natural convection in a square cavity with one sidewall heated with pulsating heat, while the opposite sidewall at a constant temperature. They demonstrated that at relatively high Rayleigh numbers, where convective heat transfer was dominant, the buoyancy driven flow had the tendency to resonate with the periodic heat supplied to the sidewall. This resonance behavior became more evident as the Rayleigh number increased. In the subsequent papers, Anthoe and Lage examined the effects of the Prandtl number and amplitude of pulsating heat on natural convection in a cavity numerically [21,22] and experimentally [23]. Their results indicated that the heat transfer across the enclosure could be either enhanced or hindered by the periodic heat.

The numerical work of Abourida et al. [27] considered the transient natural convection of a square cavity filled with air with horizontal walls submitted to periodic temperatures or heated from below. Finite difference procedure was used in the computation. The results showed that the heat transfer could be enhanced or reduced with various heating modes, periodic temperatures, and the Rayleigh number. Poujol et al. [28] studied experimentally and numerically the transient natural convection of silicon oil in a square cavity heated by a time-dependent heat flux on one vertical wall and maintained the opposite wall at a constant temperature. Temperatures at the boundary and inside the cavity were measured by thermocouples. Velocity profiles from experimental visualization were compared with the results from numerical model. However, because of the poor quality of the images from experiments, only qualitative trends could be detected, and a quantitative description is not possible. Fu and Shieh [29,30] numerically studied the natural convection in an enclosure induced simultaneously by gravity and vibration, as well as the effect of vibration frequency on transient thermal convection. The boundary layer flow induced by periodic gravity acceleration in porous media was also considered.

Oscillating convective flows recently have found applications in space-based melting processing systems under the influence of g-jitter or gravity perturbations [31], which in many cases may be represented by a Fourier series of harmonic components. However, most of the literatures discussed above focused on the effect of oscillatory driven forces on the heat transfer rates across the cavity, relatively little attention has been given to the flow

pattern that has direct implications to the solute redistribution and segregation in melt processing systems. Also, the oscillating flow behavior as a function of the Strouhal number is yet to be fully appreciated. Furthermore, the different roles played by modulated gravity or modulated temperature gradients are not well understood; for instance, question of whether a modulated thermal gradient can be used to simulate the modulated gravity remains essentially eluded. These issues are of both fundamental and practical significance. The aim of the present work is to study, by both experimental measurements and finite element modeling, the temperature distribution and flow motion driven by thermal or gravitational oscillation of various Strouhal numbers and in fluids of various Prandtl numbers. The intention is to provide a better understanding of the above issues through both measurements and simulations. Also, with the experimentally verified numerical model, assessment is made of the conditions under which some of the basic oscillating g-jitter behavior can be simulated in terrestrial environments. Due to the high cost of direct study of g-jitter effects on the thermal and fluid flow behavior in a space environment and the extreme difficulty of repeating such experiments, numerical models that are validated by obtainable experiments are essential for planning and designing thermal fluids experiments under g-jitter conditions for space processing applications.

For this purpose, a rectangular cavity of $18 \times 20 \times 150$ $(L \times H \times D)\,\mathrm{mm}^3$ in size was considered. The depth (D) of the cavity was so chosen that the three-dimensional effect may be neglected, based on the analysis of Roppo et al. [3]. The transient natural convection driven by sinusoidal wall temperatures was investigated both experimentally and numerically. Oscillating frequencies ranging from 0.02 Hz to 0.05 Hz were studied. A laser-based PIV system was used to quantitatively visualize the flow pattern. Numerical simulations were carried out using measured temperature data. The convective flow patterns as well as amplitude of velocity were compared between experimental measurements and numerical computations. With the finite element method so checked with the measurements, numerical simulations were conducted on liquids of various Prandtl numbers for a series of oscillation frequencies. Also, oscillatory temperature- and gravity-driven flows of a fluid with Prandtl number equal to 0.01 were compared. Results showed that gravity perturbation on a typical liquid metal in a microgravity environment could be simulated and studied by thermally induced, buoyancy force driven oscillation in the terrestrial environment.

2. Problem statement

Fig. 1 schematically illustrates the model system being studied along with the coordinate system for analyses.

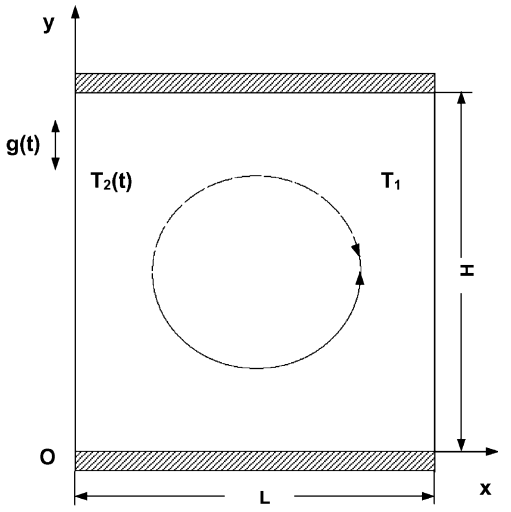

Fig. 1. Schematic representation of temperature or gravity driven oscillatory convection in a 2-D cavity.

We consider a rectangular cavity filled with distilled water. The top and bottom surfaces are adiabatic. The right side is kept at a constant temperature T_1^* and the left side is undergoing a sinusoidal temperature perturbation $T_2^*(t^*)$. The height of the cell is L^*, as non-dimensionalized, equals to 1; and the width of the cell is $0.9L^*$. The origin of the coordinate system is selected at the lower left corner of the cavity. As a result of time-varying thermal gradients, time-varying natural convection arises in the cavity. The present study is concerned with the time-varying flows induced either by an oscillating temperature field or by oscillating gravity forces.

2.1. Governing equations and numerical solutions

The fluid flow and heat transfer in the cavity are governed by the continuity equation, the Navier–Stokes equations and the energy balance equation. For the current system, when the temperature is modulated at constant gravity, these equations can be written in the dimensionless forms as follows:

$$\nabla \cdot \mathbf{u} = 0 \tag{1}$$

$$\frac{\partial \mathbf{u}}{\partial t} + (\mathbf{u} \cdot \nabla)\mathbf{u} = -\nabla p + \nabla^2 \mathbf{u} - Gr\,T(t)\,\mathbf{e} \tag{2}$$

$$\frac{\partial T}{\partial t} + \mathbf{u} \cdot \nabla T = \frac{1}{Pr}\nabla^2 T \tag{3}$$

In the above equations, lengths are non-dimensionalized by L^*, velocity by ν/L^*, time by L^{*2}/ν, frequency by ν/L^{*2}, pressure by $L^{*3}/\rho_0\nu^2$; the non-dimensional temperature is defined as $T = (T^* - T_1^*)/(T_2^* - T_1^*)$. Also use has been made of the Boussinesq

approximation $\rho(T^*) = \rho_0(1 - \beta_T(T^* - T_1^*))$, and $|\mathbf{g}|$ is equal to 1 as it is non-dimensionalized by the factor $g_0^* = 9.8\,\mathrm{m/s^2}$. The corresponding boundary conditions are as follows: $\mathbf{u} = 0$ at all boundaries, $\partial T/\partial y = 0$ at $y = 0$ and $y = 1$, $T = 0$ at $x = 0.9$, and $T = \sin(2\pi ft)$ at $x = 0$.

For the cases where the whole cavity is under a gravity perturbation, $\mathbf{g}^*(t^*) = g^*\sin(2\pi f^* t^*)\mathbf{e}$ with constant temperatures at vertical walls, the governing Navier–Stokes equation changes to:

$$\frac{\partial \mathbf{u}}{\partial t} + (\mathbf{u}\cdot\nabla)\mathbf{u} = -\nabla p + \nabla^2\mathbf{u} - Gr\,T\mathbf{g}(t) \tag{4}$$

where $\mathbf{g}^*(t^*)$ is non-dimensionalized as $\mathbf{g}(t) = g\sin(2\pi ft)\mathbf{e}$. Note that g is non-dimensionalized by the gravity constant g_0^*.

The corresponding temperature boundary conditions at two sidewalls are modified correspondingly: $T = 0$ at $x = 0.9$, and $T = 0$ at $x = 0$. The other boundary conditions remained the same.

The above equations and boundary conditions are solved using the Galerkin finite element method. The detailed description of the finite element formulation and numerical procedures is given elsewhere [31,32], and hence omitted here. The calculations used the temperatures directly measured during experiments to make a fidelity comparison. The finite element mesh consists of 900 four-node elements as shown in Fig. 2. This mesh is selected based on the mesh sensitivity study as discussed in those references. The pressure is modeled using the penalty method, along with an implicit time differencing scheme for a time matching solution.

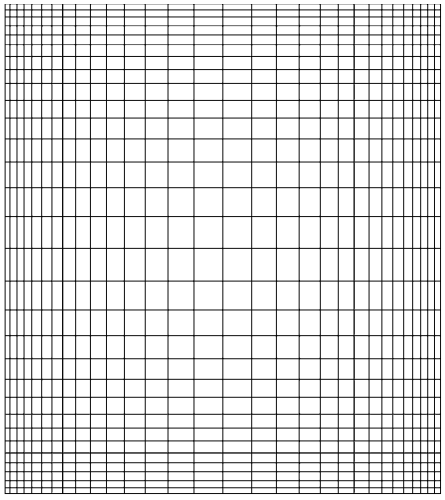

Fig. 2. Finite element mesh for mathematical model (900 four-node elements).

3. Experimental setup and procedures

3.1. System setup

The experimental system for the study of the effect of thermally driven oscillatory convection is schematically sketched in Fig. 3. The main part of the system is the rectangular cavity. The top and bottom walls of the cavity are made of 1.27 cm thick acrylic. Also 1 cm thick polystyrene is glued on these walls for insulation purpose. The two vertical sidewalls of 3.16 mm thick are made of copper for good heat conduction. They are painted dull black on the inside surfaces to reduce light reflection and glare. The working fluid is distilled water.

To generate a temporally oscillating temperature gradient across the test cell, the temperature of one vertical sidewall is maintained constant while the temperature of the other sidewall is modulated sinusoidally around an average temperature. To achieve this, the outside surface of the right wall is heated by circulating hot water from a thermostatically controlled water bath. This water bath can be maintained at constant temperature ranging from −30 °C to +100 °C. The left sidewall is heated by a Kapton flexible heater strip (Omega, Inc.) glued to its surface. This heater has a heating capacity of 1.6 W/cm^2 and is supplied with sinusoidal electrical power with the prescribed frequency from an AC amplifier driven by a signal generator installed in a computer. The excess heat from the wall is removed by circulating water from a second thermostatically controlled water bath with an operating temperature range of −50 °C to +250 °C and temperature stability of ±0.01 °C. This is needed to control the heat input so that the heated wall temperature oscillates around the mean temperature. The construction of the test cavity and the heating arrangement are described in great detail in two recent theses [33,34].

3.2. Instrumentation and data acquisition

The temperatures of the two sidewalls were measured by Type T copper-constantan thermocouples, with five thermocouples mounted on the left sidewall and two on the right sidewall, as shown in Fig. 3. The thermocouple signals were amplified, digitized and acquired by a PC equipped with a 32-channel, 16-bit Analog/Digital Converter board (Computer Boards, Inc.). The electronics used had the capability to resolve temperature to 0.005 °C. The thermocouples were calibrated against a HP 34420A nano-voltmeter (HP Co.). Details of data acquisition and thermocouple calibrations can be found in Higgins [33]. A rigorous determination of the response time of the temperature measurement system was not made in this study but, from past experience, it seems reasonable to assume that at the "medium" fre-

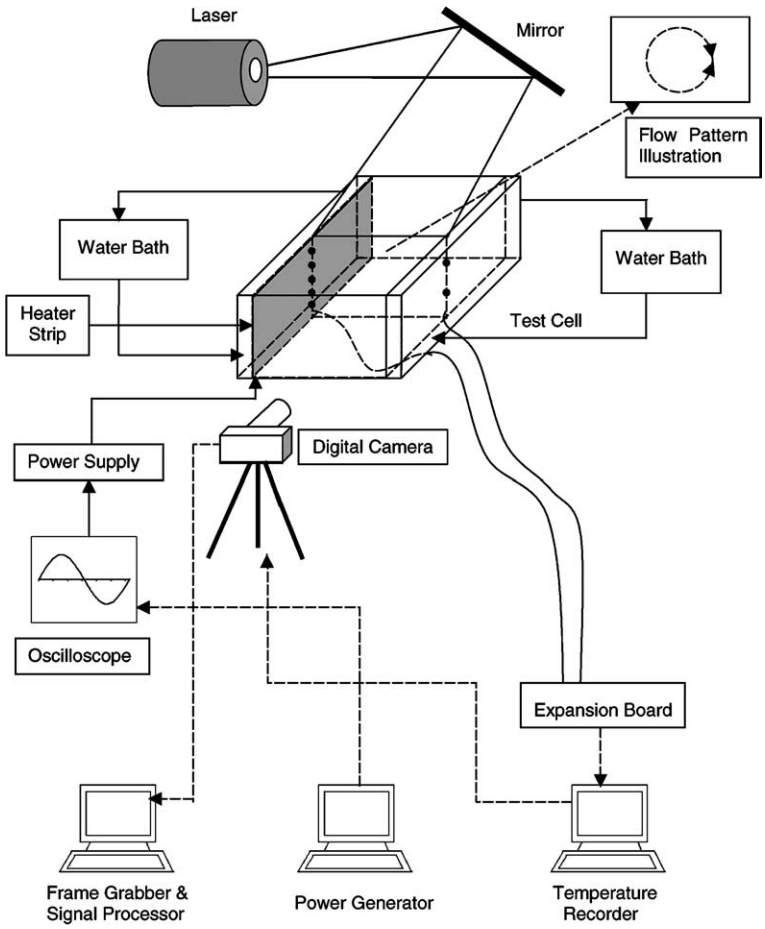

Fig. 3. Schematic diagram of the particle image velocimetry (PIV) experimental system setup.

quencies (0.01–0.05 Hz) studied, the instrumentation does not have response limitations.

The PIV system used in this experiment included three parts: the laser sheet light optics, the image recording equipment (CCD camera) controlled by a PC, and the analysis software (Insight NT). The sheet light optics consists of a 2-W Spectra-Physics argon laser, a right-angle mirror and a cylindrical lens. The Model 630044D PIVCAM 4-30 CCD video camera from TSI Inc. offers 748×486 pixels resolution and has a maximum frame rate of 30 frames per second. The resolution and speed are adequate for capturing time-sequenced images at the small flow velocities studied in the present experiments. The PC-based PIV system allows the images to be acquired at the required instants either from internally generated or externally provided trigger commands. It provides three acquisition modes to control the camera, viz., focus mode, single frame mode and sequence frame mode. Focus mode is very useful for setting up the experiment, focusing camera and displaying live video. It displays images continuously and refreshes the images at the maximum camera acquisition speed. Single frame mode is used to acquire only one frame at a time. Sequence mode is used to store the images in real time experiments. The time file created after the images are stored is used for post-processing and analysis.

Since the laser light is continuous in the present experiments, an external signal was programmed to control the camera exposure. For the low velocities involved in the experiments, the frame rate was set at two per second and the camera exposure was selected to be 200 ms between two frames.

The oscillatory heat of the left sidewall and the acquisition of images and temperature data are controlled by three PCs as shown in Fig. 3. The function of the computer on the right is to collect temperature data and to control the shutter of the CCD camera for flow visualization and PIV measurements. Two integrated circuit boards (CIO-DAS 1402/16 and CIO-CRT05, both from Computer Boards Inc.) are installed in the computer, with the former for analog/digital conversion, and the

latter for the control of shutter speed of the CCD camera. The middle computer is to control the power to heater strip mounted on the left sidewall. It uses its own counter board and sends signals to the AC power generator (Model XHR 150-7 from XANTREX Company) to generate the oscillating voltage required to produce an oscillating temperature field. The computer on the left is a dual-processor PC, designed to perform data-intensive computations for image processing. It combines image capturing and image processing into one unit. Its high speed and large memory makes it possible to save the images as fast as needed for our applications. This computer is synchronized with the computer on the right to obtain the temperature and velocity information at the same time.

The post-processing software, Insight-NT, is used to analyze the images. This software can generate vector plot data for the graphics software TECPLOT to reproduce the velocity vector field. There are many processing options available such as auto-correlation, two-frame cross-correlation, one-frame cross-correlation, adaptive auto-correlation and adaptive cross-correlation. In the present case, the most convenient option is two-frame cross-correlation. In this mode, the data from two sequential frames are compared and a vector file of velocities is obtained, from which the instantaneous direction and magnitude of the velocity at each spatial location in the flow are obtained.

Proper particle seeding of the flow field is very important to get an accurate description of the fluid motion. First, the seeding particle should have nearly the same density as the working fluid so that it can be neutrally buoyant. Secondly, the concentration of the particles within the fluid is critical. Too many particles within a small volume would blur the image and too few particles would result in poor spatial resolution of the velocity field. In the present experiments, distilled water is used as the working fluid in the test cell. The seeding particles used are 30 μm resin particles with a specific gravity of 1.02 with the concentration of particles being about 6×10^{-5} g/ml. Previous studies [33] have established the adequacy of these seeding conditions for the successful and accurate measurement of the flow velocities in the present test setup.

The estimated uncertainty in velocity measurements is ±0.04 mm/s. The resolution of each of the x and y components of the velocities is 0.60 mm × 0.67 mm in space and 200 ms in time. The present test set up gave ΔT modulation of about 2 °C in amplitude and sinusoidal within ±0.03 °C at the frequency of 0.025 Hz. The heat loss to the environment is estimated to be less than 0.5% of the heat conducting between the hot and cold walls. All the PIV images reported below were taken in the middle plane of the test cell, as shown in Fig. 3. Additional experiments were also made for vertical cross-section at two lateral locations (1.25 cm before and after the middle plane). The measurements in all these cross-sections at different lateral locations are the same, indicating that the two-dimensional pattern is sustained in the system as predicted by the theoretical analysis [3].

3.3. Experimental procedures

Before any measurements were taken, the water was allowed to flow through the water baths for about half an hour to establish a steady state. The temperature along the two sidewalls was continuously monitored. Then the required frequency of heating was tuned on. Preliminary trials showed that after 5–6 cycles, the temperature and the fluid flow reached an acceptably periodic state. For the current study, $f^* = 0.025$ Hz, both the flow and temperature gradient can be expected to become periodic within about 4 min. However, additional 30 min or more were allowed before starting to collect temperature data and the images.

4. Results and discussion

4.1. Experimental measurements and numerical simulations at $f^* = 0.025$ Hz

Fig. 4 shows the measured results of temperature variations with time as measured by all the thermocouples 1–7 used. Fig. 5 shows, for three specific instants during one thermal cycle ($t^* = 0$–40 s), the measured velocity field directly analyzed by INSIGHT-NT (#1), the corresponding convection patterns reproduced by Tecplot (#2), and the computed velocity profiles (#3) for the oscillation frequency of 0.025 Hz. The magnitude of the maximum velocity in the flow is indicated at the bottom of the figure in each of the cases (#1) and (#3). An

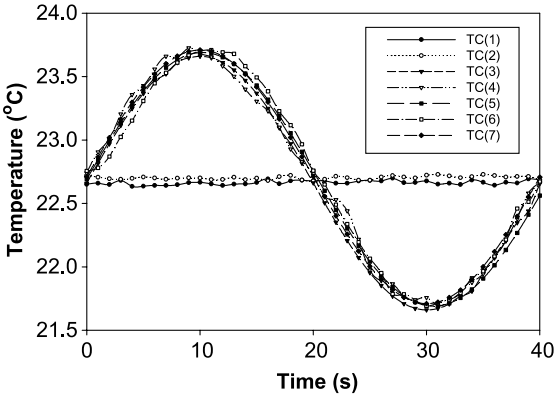

Fig. 4. Measured temperature evolution on the sidewalls of the cavity ($f^* = 0.025$ Hz). The number in the legend represents the thermocouple series. TC(1) and TC(2) are thermocouples on the right sidewall and TC(3)–TC(7) are on the left sidewall.

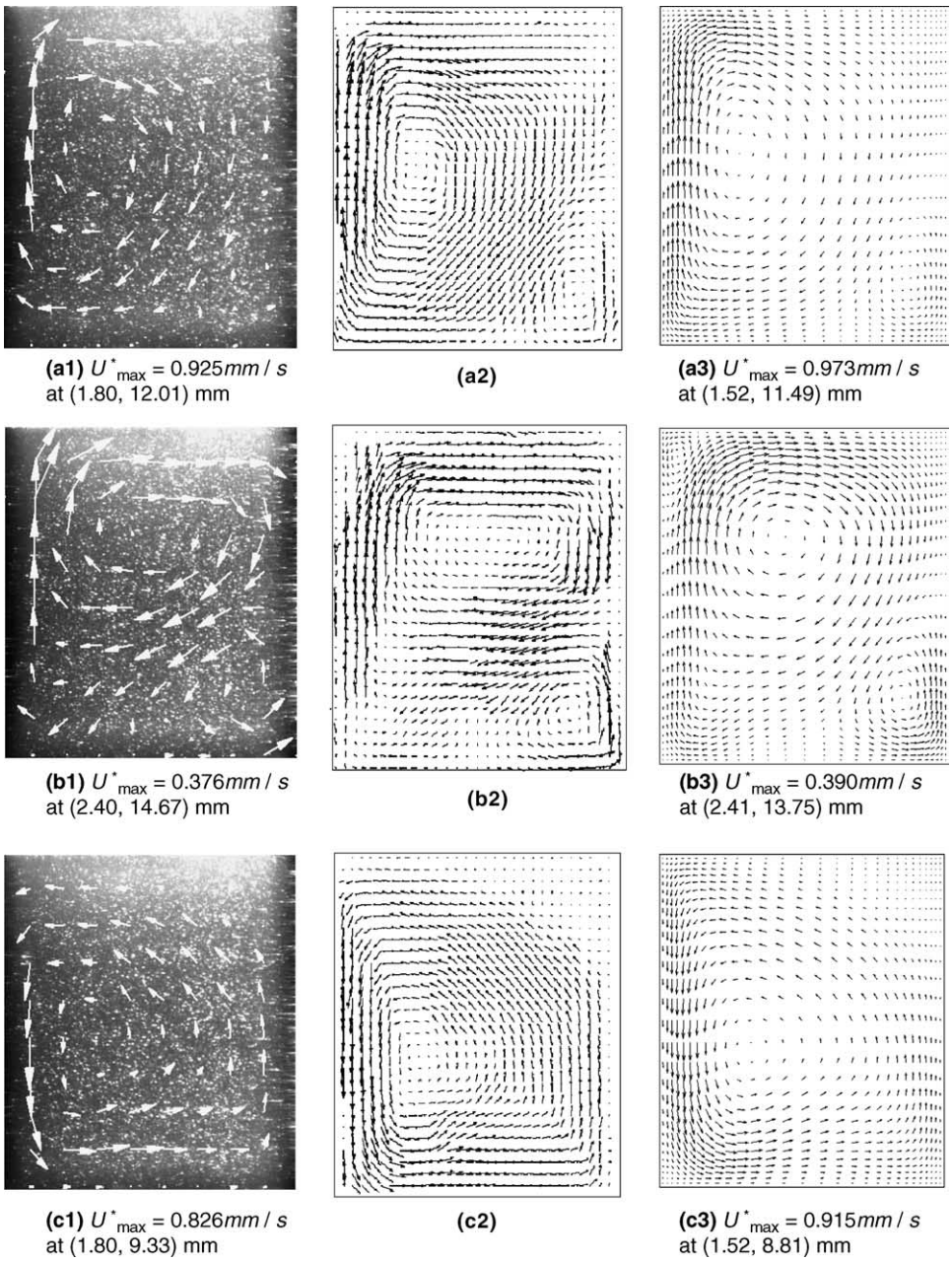

Fig. 5. Dynamic development of velocity fields driven by oscillating temperature gradients (f^* = 0.025 Hz) within one thermal cycle, as measured by the PIV system and computed by numerical model. The plot region is 18 mm × 20 mm. Column #1 are images analyzed by Insight-NT, column #2 by Tecplot, and column #3 by numerical model. (a) t^* = 13.6 s, (b) t^* = 23.6 s, and (c) t^* = 37.6 s.

examination of these figures shows that the experimental measurements and the numerical simulations are in excellent agreement both qualitatively and quantitatively, within the uncertainty of the measurements. The difference between the maximum velocities is 0.048–0.089 mm/s, which compare with the resolution accuracy of 0.04 mm/s (see Section 3). The difference in locations where these maximum velocities occur is 0.3–0.92 mm, which is also compatible with the uncertainty of the spatial resolution of the PIV system (0.67 mm, see Section 3). As the flow is transient and evolves in time, only some of the snapshot pictures can be presented here. Nonetheless, these snapshots reveal some of the very essential features of periodic convection in the system. Both the measured

and computed results show that the liquid convection in the cell responds to the temperature changes in time. A large convection cell is developed initially ($t^* = 13.6$ s), circulating down along the right wall and moving upward along the left wall, as shown in Fig. 5a1–a3. The center of this large flow cell is located closer to the left wall to satisfy the mass conservation across the liquid pool. It is noticed that the flow near the left wall shows a high velocity magnitude and it gets weaker near the right wall at this instant. Near the lower corner of the right wall, a smaller, weak, and counter-rotating eddy develops and appears to contribute to the weakening of the convection along this wall.

At the next instant in time ($t^* = 23.6$ s), the convective flow structure evolves to a different stage and the large recirculating cell moves upward, as indicated by the displacement of its center, while the smaller, counter-rotating flow cell starts to grow in size and gain in strength. This is clearly shown in Fig. 5b1–b3. Notice that the vectors plotted are enlarged so as to clearly show the flow structure at this instant. As such, a smaller reference velocity vector is used for the plot.

The convective flow field continues to evolve in response to the temperature change in time. The weaker and smaller cell appearing at the low corner of the liquid pool, as shown in Fig. 5a1–a3, continues to grow in strength and invades into the territory of the large cell. As the temperature of the left wall decreases below the right wall temperature, the initially small cell spreads across the entire liquid pool, reversing the global flow structure completely. This is clearly seen in Fig. 5c ($t^* = 37.6$ s) where the instantaneous temperature of the left wall is actually lower than the right wall temperature, thereby causing the flow to reverse. There appears to be a rather weaker and smaller flow cell developing at the upper corner near the right wall.

Comparison of measured and calculated velocities at two specific locations, nodes #1 and #2, as evolving in time, is illustrated in Fig. 6. Evidently, there is very good agreement between the experimental measurements and numerical model predictions. For the sake of comparison, the modulation of the driving temperature difference during this cycle is reproduced in this figure from Fig. 4. It is clearly seen that there exists a phase lag in the response of the local velocity relative to the temperature modulation and that this phase difference varies across the cavity from node #1 to #2. This confirms our previous studies [31,32,35–37], which also indicated that the phase difference depends on many factors, such as location, applied temperature difference and modulation frequency.

From the experimental measurements and computed results for other conditions, it is found that the convection pattern and flow oscillation are strong functions of applied frequency and are also dependent upon the orientation of the liquid cell with respect to gravity. The orientation effects are shown in a set of snapshots of the measured and computed results at various instants for a 45° tilted configuration, where gravity points downwards (see Fig. 7). The temperature modulation is shown in this figure. Clearly, the measured and computed results for this configuration are once again in agreement for both flow patterns and velocity magnitudes. The oscillating flow structures, in response to the time evolution of the thermal environment, are very similar to those presented above when gravity is perpendicular to the temperature gradient. However, both the measured and computed results show some subtle and yet important differences between the two configurations, as contrasted in Fig. 7c and Fig. 5b which have the same temperature boundary conditions. In Fig. 7c, the flow field is characterized by three flow cells, with two large ones, approximately equal in size and strength,

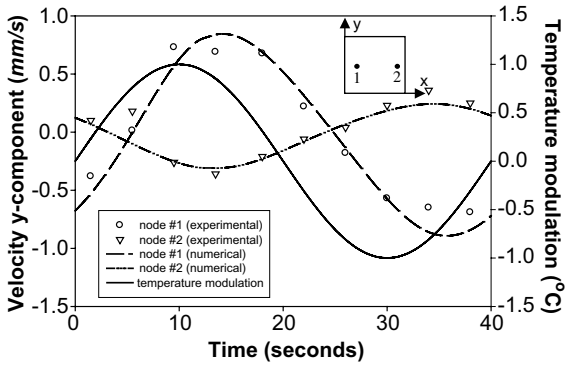

Fig. 6. Comparison of measured and calculated velocity y-component at two different locations in the test cavity within one cycle at $f^* = 0.025$ Hz. The coordinates of node #1 are (1.9 mm, 10.0 mm) and the coordinates of node #2 are (16.01 mm, 10.0 mm), all measured from the lower left corner of the cavity. The temperature modulation between two sidewalls is also plotted to show the phase angle.

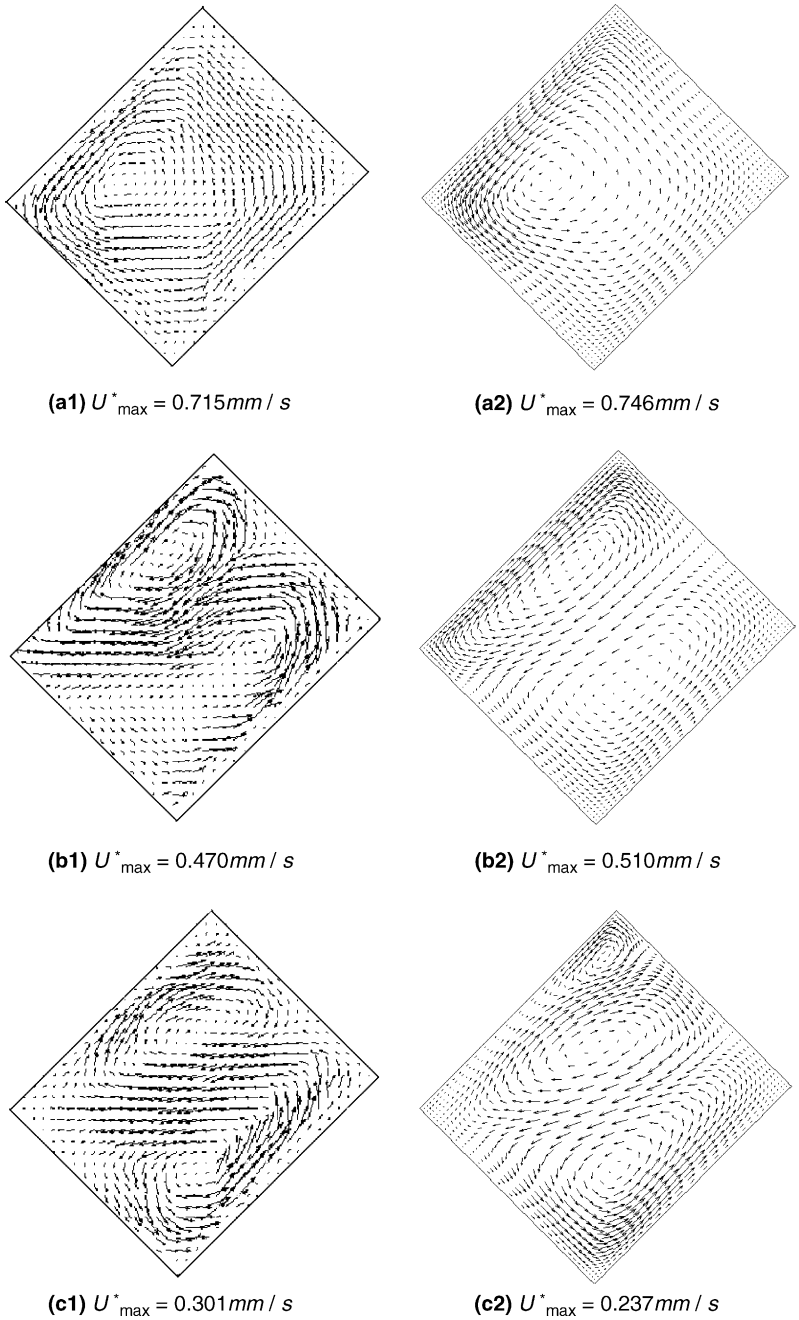

Fig. 7. Comparison of transient development of oscillating velocity profiles measured by the PIV system and by the finite element model for the configuration tilted at 45° ($f^* = 0.025$ Hz). The plot region is 18 mm × 20 mm with the hot wall on top. (a1,b1,c1) are experimental results plotted by Tecplot and (a2,b2,c2) are numerical simulations. (a) $t^* = 0.2$ s, (b) $t^* = 12.4$ s and (c) $t^* = 23.6$ s.

occupying the entire liquid pool and a small one appearing at the upper corner of the hot wall. In contrast, for the same temperature gradient, though there are still three cells (as seen in Fig. 5b), only the large one occupies the major portion of the liquid pool. Besides, there is one small counter-rotating vortex at the cold bottom part of the cavity and an even smaller eddy barely noticed at the upper corner of the hot wall. The maximum velocities also differ by about 30% for the two cases.

Experiments were also conducted with an inverted cavity. At this condition, the two sidewalls are insulated by 1 cm thick polystyrene. The bottom wall is at a fixed

temperature while the temperature of the top wall undergoes an oscillation with a frequency equal to 0.025 Hz and amplitude about ±1.0 °C. The maximum Rayleigh number for this configuration is about 1.2×10^5, which is well above the critical Rayleigh number of ~4000 for the onset of convection in a nearly square enclosure [38]. It is noted that the critical *Ra* cited here is for a cavity with a constant inverted temperature gradient and it is thus used as a reference for the present case, since the exact critical *Ra* for the case with oscillating temperatures is not available. In general, the critical *Ra* number will be somewhat different when an oscillating temperature gradient is imposed and the sidewalls are insulated [5]. Analysis of the data shows that the maximum velocity oscillates ±0.10 mm/s around 0.5 mm/s, which is attributed to the changes in driving force. However, the cell pattern remains unchanged with the temperature perturbation, despite of the oscillating temperature gradients applied between the top and bottom walls. Therefore, results are shown for only one instant of time in Fig. 8. The top one is the image analyzed by Insight-NT, and bottom one is the vector file read by Tecplot. For this case, the experimental measurements indicate mainly two counter-rotating flow cells, equal in size and strength, which are recirculating in the entire liquid pool. Also there are some small eddies near the top wall. However, the trend is not very clear. The detailed analysis of this case would require different numerical treatment, which is beyond the scope of this paper.

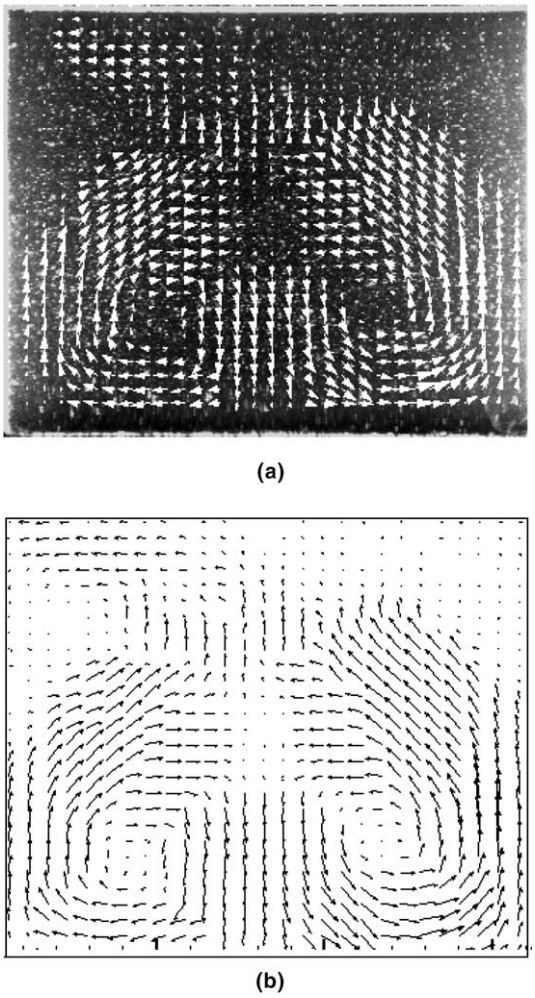

Fig. 8. Convective flow patterns of water in an inversed cavity driven by oscillating temperature gradients ($f^* = 0.025$ Hz). Plot region is 20.0 mm × 18.0 mm. $U^*_{max} = 0.578$ mm/s. (a) Image analyzed by Insight-NT, and (b) vector file read by Tecplot.

Fig. 9 shows the numerical predictions of the change in amplitude of velocity with respect to the Strouhal number for the upright cavity in the range $0.01 < St < 30$. Experimental results obtained at frequency $f^* = 0.02$ Hz, 0.025 Hz, 0.033 Hz and 0.05 Hz have been non-dimensionalized and plotted on the same graph. The experimental measurements data fall into the numerical curve and have the same tendency with that of numerical simulation at the overlap region $St = 0.5$–5.

4.2. Numerical simulation of flow oscillation at different frequencies and Prandtl numbers

Using the mathematical model validated by the experimental measurements as described previously, numerical simulations were conducted with the same boundary conditions and configuration as experiments. All the results showed below are dimensionless. Strouhal numbers varying from "very low" (quasi-steady, $St = 0.01$) to "very high" ($St = 30$) were considered. Various Prandtl numbers were selected to simulate different types of fluids.

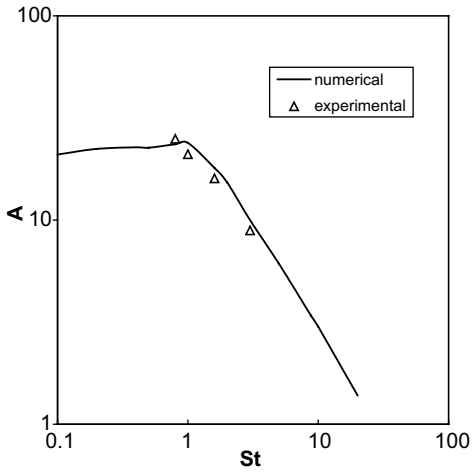

Fig. 9. Measured and calculated results of amplitude of velocity oscillation vs. the Strouhal number for distilled water. $Pr = 6.13$.

As shown in Fig. 10, the amplitudes of flow oscillation decrease sharply with Strouhal numbers, especially in the range $1 < St < 30$ in most of the cases. The reason for this trend is that at the high frequencies, the viscous boundary layer is very thin and hardly felt by most of the fluid in the cavity. This prediction is in agreement with the analytical "Stokes-flow" solution for the oscillating plate [39]. However, there is noticeable difference between low Prandtl number and high Prandtl number cases with respect to the effect of frequency in the low-to-medium range. Fluids with small Prandtl number typical of liquid metals exhibit a consistent tendency in the whole domain, i.e., amplitude of velocity decreases with the Strouhal number. For medium to high Prandtl number fluids, however, there exists a maximum amplitude around $St = 1$. At lower Strouhal numbers, the non-linear convection terms in the governing equations begin to have a very strong effect on the flow pattern within the cavity. Aspect ratio (L/H) of the cavity also plays an important role under this condition. Due to the confined domain of the cell, there is an interaction between the viscous boundary layer on the left and the flow field on the right. At small Strouhal numbers, the viscous boundary layer thickness will be comparable to the width of the cavity, thus affecting the main flow field. That this indeed is the case was seen from the results obtained when aspect ratio was increased to 5 in calculations at $St = 0.01$ and $Pr = 6.13$. Results showed that the amplitude of velocity increased from 15.3 to 20.9. Hence, in a finite cavity, the strength of fluid flow induced by temperature oscillation is a function of Prandtl number, Strouhal number and the aspect ratio of the cavity.

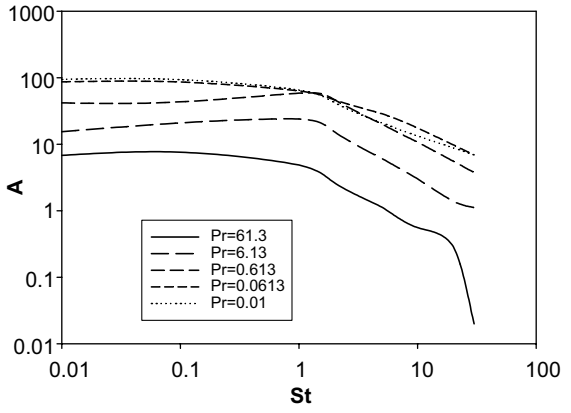

Fig. 10. Numerical predictions of amplitude of velocity modulation changing with Strouhal number for different Prandtl number fluids.

Fig. 11 shows the instantaneous temperature distributions across the test cell (in the mid-plane $y = 0$) at four time instants, $\omega t = 0$, $\omega t = \pi/4$, $\omega t = \pi/2$, and $\omega t = 3\pi/4$ during the oscillation cycle. These are shown for a fixed St (1.0) but for two different Pr. These calculations showed that the temperature distributions

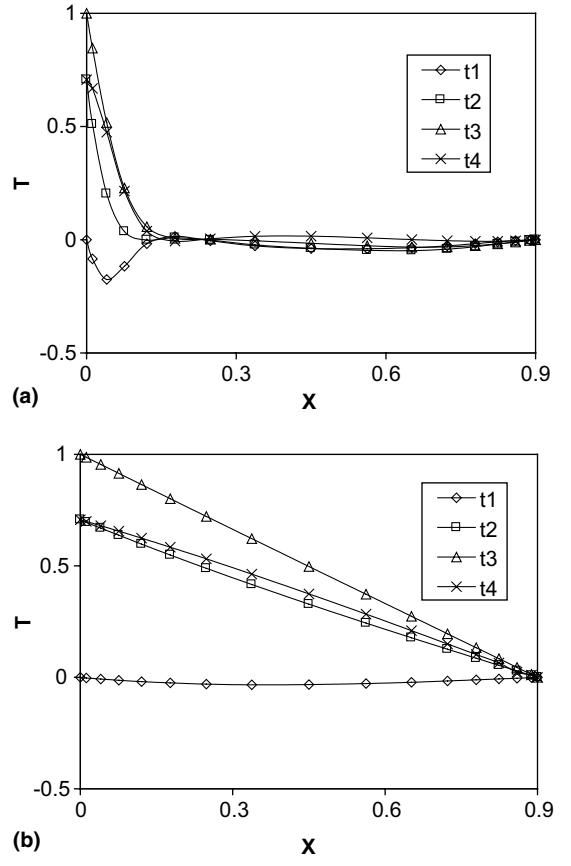

Fig. 11. Temperature distributions along $y = 0$ within the cavity at different time instants at $St = 1$. $\omega t_1 = 0$; $\omega t_2 = \pi/4$; $\omega t_3 = \pi/2$; $\omega t_4 = 3\pi/4$. (a) $Pr = 6.13$, and (b) $Pr = 0.01$.

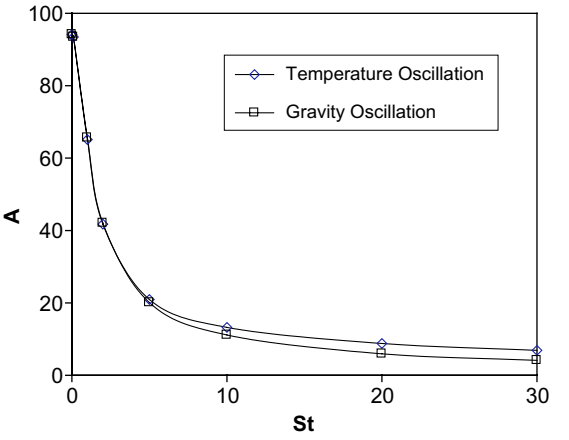

Fig. 12. Comparison of amplitude of velocity (A) vs. Strouhal number (St) in modulated gravity and thermal gradients respectively. $Pr = 0.01$.

during the latter half cycle (π–2π) are almost symmetric with the former half (0–π), and are hence not shown. Fig. 11(a) indicates the presence of a viscous boundary layer and represents the temperature distribution of water, which is the result of a combination of convection and conduction effects under the temperature oscillation at the highest Prandtl number. The nearly linear temperature distributions in Fig. 11(b) indicate conduction dominant situation at the low Prandtl number, which is consistent with the *Pr* effect on convection in porous media with temperatures oscillating at the resonance frequency [22].

4.3. Low Prandtl number fluid under either gravity perturbation or temperature oscillation

Fig. 12 is the comparison of temperature oscillation or gravity perturbation respectively for a fluid with

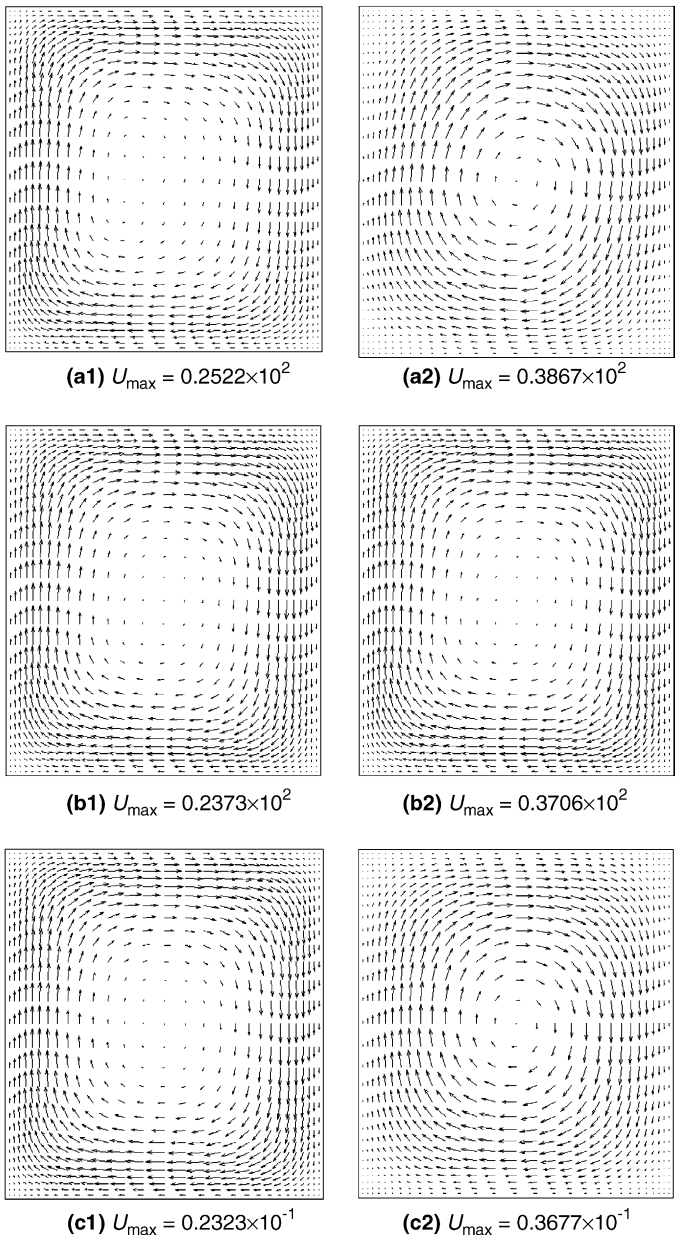

Fig. 13. Comparison of velocity fields driven by temperature oscillation, earth gravity ($\mathbf{g}_0$) oscillation and g-jitter ($10^{-3}\mathbf{g}_0$) respectively at $St = 2$. (a) Temperature oscillation; (b) Earth gravity oscillation and (c) g-jitter oscillation. (a1,b1,c1) are at time $\omega t = \pi/2$, and (a2,b2,c2) are at time $\omega t = \pi$.

$Pr = 0.01$. These results indicate that the amplitudes of flow field are attenuated with the increase in frequency. Lower frequency oscillations of gravity perpendicular to the temperature gradient have a stronger effect on the flows than higher frequency oscillations. Also, modulated gravity and modulated temperature have almost the same effects on flows in a cavity for small Prandtl number fluids, which are typical of molten metals and semiconductors, especially in the low frequency range.

Figs. 13 and 14 provide further evidence showing that g-jitter perturbation in microgravity environments can be simulated adequately by buoyancy driven flow in ground-based experiments. Fig. 13 shows a comparison of the velocity profiles driven by temperature oscillation, earth gravity oscillation and g-jitter perturbation respectively. The detailed information on the distribution of amplitude of velocity oscillation along $y = 0$ is shown in Fig. 14. The flow tendencies and the magnitude of the amplitude are identical in all these cases.

Real g-jitter is random in nature as the results of mechanical vibration, atmospheric drag, terrestrial gravity gradients, etc. Numerical simulation of water was carried out using these g-jitter data. Since there is no regularly driven force, the convective flows in the system must be monitored at every instant. These results showed similar flow patterns compared with those of temperature driven oscillation or single-frequency gravity perturbations, with one recirculating loop (see Fig. 15a). However, the time evolution of velocity at some specific locations (Fig. 15b and c) illustrates that the velocity responds quickly with respect to g-jitter, which is consistent with our previous results on a binary alloy [31].

These results further prove that introducing thermally induced buoyancy force oscillation in a terrestrial environment drives the flow in a manner similar to gravity fluctuation in microgravity environments.

5. Concluding remarks

In this paper, natural convection in a cavity driven by oscillating temperature gradients or gravitational forces was studied experimentally and numerically. The numerical study is based on the finite element simulations of the temperature and velocity fields in the cavity over a wide range of frequencies and Prandtl

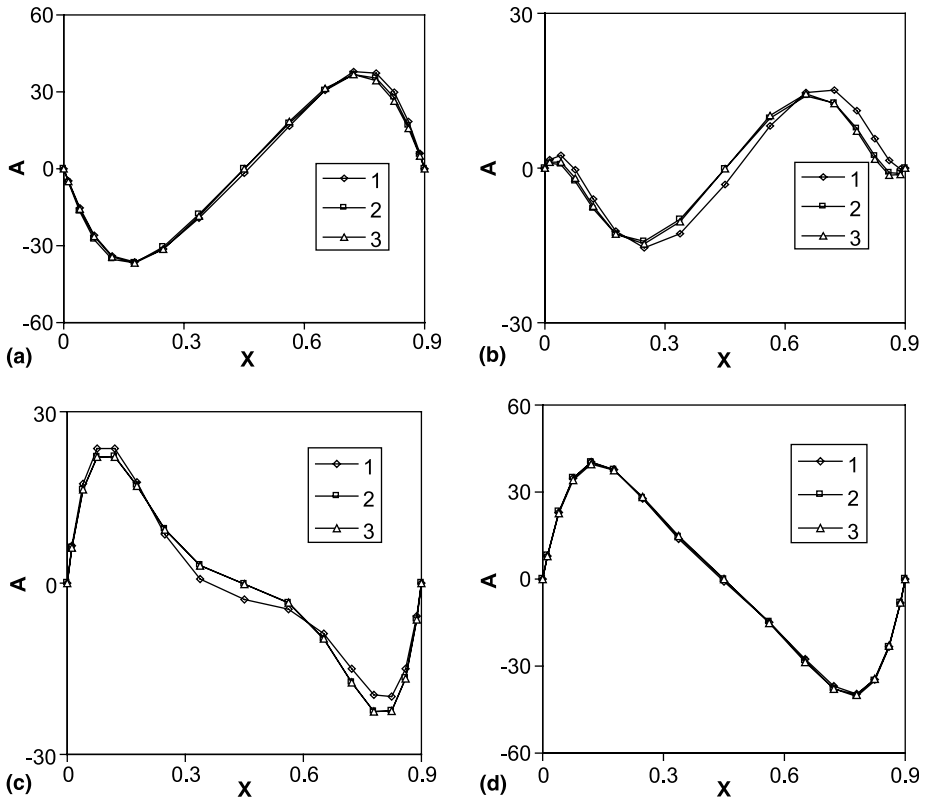

Fig. 14. Velocity distribution along $y = 0$ under temperature oscillation or gravity perturbation for $Pr = 0.01$ at $St = 2$. (a) Temperature oscillation; (b) Earth gravity oscillation, and (c) g-jitter ($10^{-3}\mathbf{g}_0$) oscillation. The amplitude of velocity driven by g-jitter is amplified 10^3 to fit in graphs. (1) $\omega t = 0$, (2) $\omega t = \pi/4$, (3) $\omega t = \pi/2$, and (4) $\omega t = 3\pi/4$.

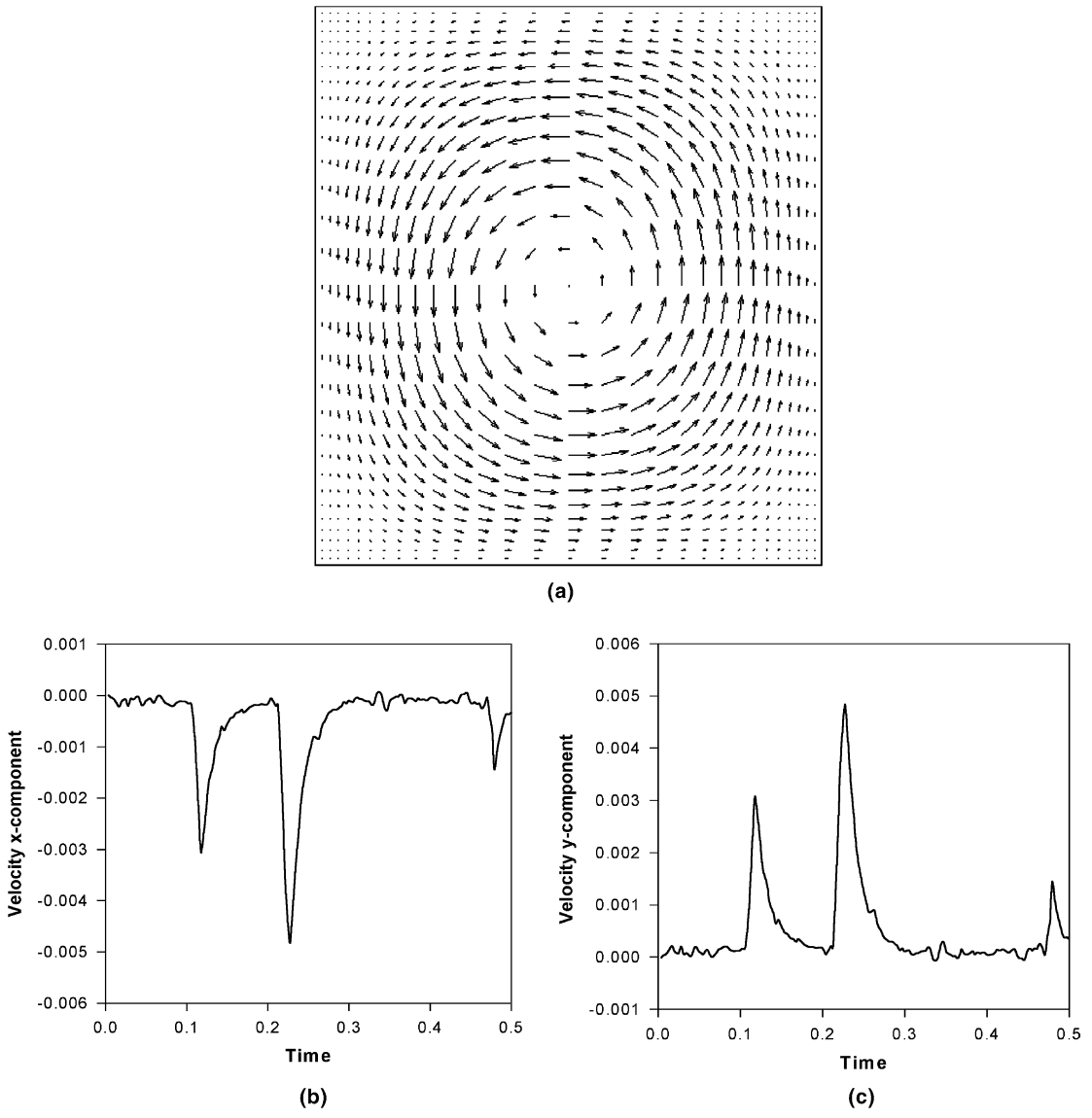

Fig. 15. Velocity profile of pure water and x- and y-components of convection driven by real g-jitter oscillation: (a) Profile at $t = 0.2698$ ($U_{max} = 0.1145 \times 10^{-2}$), (b) x-component at (0.45, 0.9367), and (c) y-component at (0.8430, 0.5).

numbers. A PIV system was set up and used to visualize the oscillating flow and to measure the convection velocity field inside the cavity with imposed oscillating temperature gradients. The following conclusions can be made based on the results obtained from these efforts.

Results for the selected modulation frequency of 0.025 Hz show that the transient thermal convection patterns approximately follow the oscillation of the driving temperature gradients. However, a phase difference exists between the driving wall temperature modulation and the resulting velocity fields. This holds true for both the vertical configuration of the cavity where the gravity is perpendicular to the thermal gradient and the tilted one where the gravity acts at an angle with the gravity.

The strength of flow oscillation in a cavity strongly depends on the frequency of temperature perturbation applied on its boundary. The flow modulation is weaker at higher frequencies of temperature oscillation.

For high Prandtl number fluids, there exists a combined contribution from non-linear convection and aspect ratio effects to the amplitude of the flow. For low Prandtl number fluids, temperature oscillation and gravity oscillation have very similar effects on the flow pattern and temperature distribution within the cavity. For these fluids, terrestrial experiments with oscillating

temperatures may be used to simulate very basic oscillatory nature of g-jitter effects on flows in microgravity.

The finite element model is in good agreement with the experimental measurements, and thus may be used both for fundamental understanding of flows driven by modulated gravity and/or thermal gradients and for design thermal systems and experiments under microgravity conditions.

Acknowledgment

Support of this work by NASA (Grant no.: NAG8-1693) is gratefully acknowledged, and so is the assistance of Mr. R. Lentz with the experimental setup and instrumentation.

References

[1] G.Z. Gershuni, E.M. Zhukhoviskii, Convective stability of incompressible fluids. Israel Program for Scientific Translations, 1976.
[2] G. Venezian, Effect of modulation on the onset of thermal convection, J. Fluid Mech. 35 (2) (1969) 243–254.
[3] M.N. Roppo, S.H. Davis, S. Rosenbalt, Bénard convection with time-periodic heating, Phys. Fluids 27 (4) (1984) 796–803.
[4] J.L. Rogers, M.F. Schatz, Superlattice patterns in vertically oscillated Rayleigh–Benard convection, Phys. Rev. Lett. 85 (20) (2000) 4281–4284.
[5] J.L. Rogers, W. Pesch, M.F. Schatz, Pattern formation in vertically oscillated convection, Nonlinearity 16 (2003) C1–C10.
[6] P.M. Gresho, R.L. Sani, The effects of gravity modulation on the stability of a heated fluid layer, J. Fluid Mech. 40 (4) (1970) 783–806.
[7] S.R. Rosenblat, D.M. Herbert, Low-frequency modulation of thermal instability, J. Fluid Mech. 43 (2) (1970) 385–398.
[8] S.R. Rosenblat, G.A. Tanka, Modulation of thermal convection instability, Phys. Fluids 14 (7) (1971) 1319–1322.
[9] C.S. Yih, C.H. Li, Instability of unsteady flows or configurations. Part 2. Convective instability, J. Fluid Mech. 54 (1) (1972) 143–152.
[10] M. Wadih, B. Roux, Natural convection in a long vertical cylinder under gravity modulation, J. Fluid Mech. 193 (1988) 391–415.
[11] R. Clever, G. Schubert, F.H. Busse, Three-dimensional oscillatory convection in a gravitational modulated fluid layer, Phys. Fluids, A Fluid Dyn. 5 (10) (1993) 2430–2437.
[12] B.Q. Li, Stability of modulated gravity-induced thermal convection in magnetic field, Phys. Rev. E 63 (2001) 041508.
[13] G. Ahlers, P.C. Hohenberg, M. Lücke, Thermal convection under external modulation of the driving force, I. The Lorenz model, Phys. Rev. A 32 (6) (1985) 3493–3518.
[14] G. Ahlers, P.C. Hohenberg, M. Lücke, Thermal convection under external modulation of the driving force, II. Experiments, Phys. Rev. A 32 (6) (1985) 3519–3534.
[15] P.C. Hohenberg, J.B. Swift, Hexagons and rolls in periodically modulated Rayleigh–Benard convection, Phys. Rev. A 35 (9) (1988) 3855–3873.
[16] C.W. Meyer, D. Cannell, G. Ahlers, Hexagonal and roll flow pattern in temporally modulated Rayleigh–Benard convection, Phys. Rev. A 45 (12) (1992) 8583–8604.
[17] M. Kazmierczak, Z. Chinoda, Buoyancy-driven flow in an enclosure with time periodic boundary conditions, Int. J. Heat Mass Transfer 35 (6) (1992) 1507–1518.
[18] H.S. Kwak, J.M. Hyun, Natural convection in an enclosure having a vertical sidewall with time-varying temperature, J. Fluid Mech. 329 (1996) 65–88.
[19] H.S. Kwak, K. Kuwahara, J.M. Hyun, Resonant enhancement of natural convection heat transfer in a square enclosure, Int. J. Heat Mass Transfer 41 (1998) 2837–2846.
[20] J.L. Lage, A. Bejan, The resonance of natural convection in an enclosure heated periodically from the side, Int. J. Heat Mass Transfer 36 (8) (1993) 2027–2038.
[21] B.V. Antohe, J.L. Lage, Amplitude effect on convection induced by time-periodic horizontal heating, Int. J. Heat Mass Transfer 39 (6) (1996) 1121–1133.
[22] B.V. Antohe, J.L. Lage, The Prandtl number effect on the optimum heating frequency of an enclosure filled with fluid or with a saturated porous medium, Int. J. Heat Mass Transfer 40 (6) (1997) 1313–1323.
[23] B.V. Antohe, J.L. Lage, Natural convection in an enclosure under time periodic heating: An experimental study, ASME-HTD 324 (2) (1996) 57–64.
[24] J.L. Lage, B.V. Antohe, Convection resonance and heat transfer enhancement of periodically heated fluid enclosures, in: J. Padet, F. Arinc (Eds.), Transient Convective Heat Transfer, Begell House, New York, 1997, pp. 259–268.
[25] J.L. Lage, Convective currents induced by periodic time-dependent vertical density gradient, Int. J. Heat Fluid Flow 15 (1994) 233–240.
[26] B.V. Antohe, J.L. Lage, Experimental investigation on pulsating horizontal heating of a water-filled enclosure, ASME J. Heat Transfer 118 (1996) 889–896.
[27] B. Abourida, M. Hasnaoui, S. Douamna, Transient natural convection in a square enclosure with horizontal walls submitted to periodic temperatures, Numer. Heat Transf. A Appl. 36 (1999) 737–750.
[28] F.T. Poujol, J. Rojas, E. Ramos, Natural convection of a high Prandtl number fluid in a cavity, Int. Commun. Heat Mass Transfer 27 (1) (2000) 109–118.
[29] W.S. Fu, W.J. Shien, A study of thermal convection in an enclosure induced simultaneously by gravity and vibration, Int. J. Heat Mass Transfer 35 (7) (1992) 1695–1710.
[30] W.S. Fu, W.J. Shien, Transient thermal convection in an enclosure induced simultaneously by gravity and vibration, Int. J. Heat Mass Transfer 36 (2) (1993) 437–452.
[31] Y. Shu, B.Q. Li, H.C. de Groh III, Numerical study of g-jitter induced double-diffusive convection, Numer. Heat Trans. A Appl. 39 (2001) 245–265.
[32] Y. Shu, B.Q. Li, H.C. de Groh III, Magnetic damping of g-jitter induced double-diffusive convection, Numer. Heat Trans. A Appl. 42 (2002) 345–364.

[33] M.K. Higgins, PIV study of oscillating natural convection flow within a horizontal rectangular enclosure, MS thesis, Washington State University, Pullman, WA, 2000.
[34] Y. Shu, Experimental and numerical studies of natural convection and solidification in constant and oscillating temperature fields, PhD thesis, Washington State University, Pullman, WA, 2003.
[35] B.Q. Li, G-jitter induced free convection in a transverse magnetic field, Int. J. Heat Mass Transfer 39 (14) (1996) 2853–2860.
[36] B.Q. Li, Effect of magnetic field on low frequency oscillating natural convection, Int. J. Eng. Sci. 34 (12) (1997) 1369–1383.
[37] B. Pan, B.Q. Li, Effect of magnetic fields on oscillating mixed convection, Int. J. Heat Mass Transfer 41 (17) (1998) 2705–2710.
[38] N.Y. Lee, W.W. Schultz, Stability of fluid in a rectangular enclosure by spectral method, Int. J. Heat Mass Transfer 32 (3) (1989) 513–520.
[39] R.L. Panton, Incompressible Flow, first ed., Wiley, New York, 1984, pp. 266–275.